Theory and Practice of Science and Technology
2025, VOL. 6, NO. 1, 172-177
DOI: 10.47297/taposatWSP2633-456933.20250601

Dynamic characteristics analysis of thin-walled parts based on mirror processing system

Xingguo Chang

School of Mechanical Engineering, Tianjin University of Technology and Education, Tianjin 300222, China

ABSTRACT
Mirror milling is an effective method for processing large thin-walled parts in the aerospace field, and vibration during the milling process is a key factor affecting the processing quality. Therefore, how to accurately predict the vibration of thin-walled workpieces during mirror milling is a key issue to optimize processing parameters and improve processing accuracy. This paper establishes a time-varying dynamic model of mirror milling stiffness of thin-walled parts based on the improved Fourier series to accurately analyze and predict the dynamic characteristics and response of the workpiece. First, for the clamping method of large thin-walled parts, springs with different stiffnesses are used to simulate the boundary conditions, and then the kinetic energy, potential energy and spring elastic potential energy of the thin-walled parts under the initial working conditions are solved, and finally the variational method is used to obtain the functional . The extreme value obtains its natural frequency. Considering the changes in the quality of thin-walled parts and the influence of the support head during the milling process, the stiffness matrix is iteratively calculated, a dynamic model is established, and the impact of stiffness changes on the frequency response function and milling vibration is accurately predicted and analyzed.

KEYWORDS
Mirror milling; Vibration; Time-varying stiffness; Predictive

1 Introduction

In aerospace and other fields, thin-walled parts have the characteristics of large size, complex shape, thin thickness, poor rigidity, etc., making them difficult to manufacture[1]. During the milling process, the interaction between the thin-walled part and the tool causes the generation of forced vibration, which is difficult to avoid during the machining process. For thin-walled part with larger thicknesses, the vibration caused by tool loading during milling is relatively small. However, due to its low stiffness, thin-walled part are prone to produce large vibrations when subjected to tool loading. This problem has become a key factor restricting the milling accuracy of thin-walled part. At present, mirror milling is an effective method for processing thin-walled parts. The main feature of this technology is that during the processing process, the milling cutter and the support device keep mirror synchronous movement. Mirror milling technology effectively suppresses vibrations generated during the machining process by increasing the local stiffness and damping near the support position of thin-walled parts, thereby improving machining accuracy. However, the accuracy of mirror milling is also affected by the vibration of thin-walled parts during processing. Therefore, how to accurately predict the vibration of thin-walled parts during mirror milling is a key issue in optimizing processing parameters and improving processing quality[2]. The vibration of thin-walled parts during the milling process has always received widespread attention. Li[3] conducted an in-depth study on the vibration response of thin-walled parts during the milling process. By constructing a multi-point contact dynamics model of the milling system, Rayleigh The Z method and Lagrange equation are used to derive the thin plate control equation, and then the analytical method is used to predict the vibration response of the milling of thin-walled parts. Bao et al[4]designed a milling test for paraffin-filled titanium alloy frame thin-walled parts, and analyzed and compared the vibration acceleration signal during the test and the quality of the machined surface. Cui[5]proposed a clamping layout strategy aimed at suppressing the machining vibration of thin-walled structures caused by cutting forces by analyzing the impact of clamping layout on the dynamic characteristics of thin-walled parts. Li Liang[6] analyzed the influence of radial milling force and milling amount on the vibration amplitude of thin-walled part machining, and verified the theoretical model through experiments. Zhang Jun[7] proposed an improved Rayleigh-Ritz method to analyze the energy changes of the plate and solve the natural frequency of the thin-walled parts for the vibration of complex thin-walled parts, which is difficult to solve. Wan Chunbo[8] constructed the relative transfer function of the milling processing system, derived a chatter stability model for thin-walled parts milling, and accurately predicted the chatter phenomenon during the milling process of thin-walled parts. In response to the vibration problem of mirror milling, Arnaud et al.[9] used finite element software and considered the material removal during the processing to study the vibration behavior of triangular thin-walled part at different positions during the milling process. Bo et al.[10] used hammering modal experiments to explore the influence of the support load in the mirror milling support structure on the modal parameters of thin-walled part.

In summary, this paper establishes a vibration analysis model of thin-walled parts under initial working conditions based on the improved Fourier series. On this basis, the stiffness changes caused by the changes in the quality of thin-walled part during the milling process are considered, and the quality and The stiffness matrix is iteratively calculated and the modal transformation is performed to obtain the dynamic prediction model during the milling process. Finally, the model prediction results are compared through the hammering modal test and the mirror milling test to verify the accuracy of the model.

2 Time-varying dynamics model for mirror milling of thin-walled parts

2.1 Theoretical modeling of vibration of thin-walled parts under initial conditions

In order to better simulate the boundary conditions, the displacement spring and the rotating spring are used to impose constraints. As shown in Figure 1, The stiffness of the two springs are k and K respectively. l_x represents the length of the thin-walled part, l_y represents the width of the thin-walled part, h represents the thickness of the thin-walled part, and S represents the area of the thin-walled part. Only consider the bending effect of the thin-walled part and ignore the mass of the spring. The kinetic energy of the thin-walled part under the initial working condition as:

$$T_0=\frac{1}{2}\rho h \,{}_{s}\left(\frac{\partial w}{\partial t}\right)^2 ds \tag{1}$$

where w represents the displacement of the thin-walled part in the z direction.

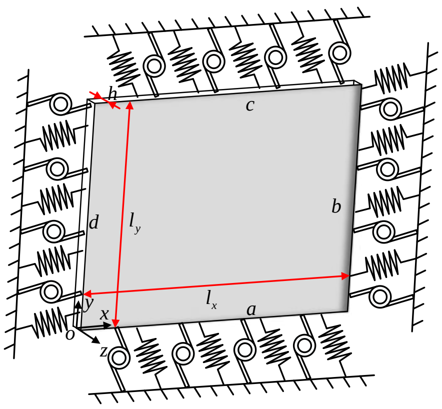

Figure 1 Theoretical model of thin-walled parts under arbitrary boundary conditions under initial conditions

The displacement function of thin-walled parts is:

$$w(x,y,t)=\sum_{m=1}^{M}\sum_{n=1}^{N} A_{ij}\varphi_i(x)\varphi_j(y)\; e^{iwt} \tag{2}$$

In the formula, M and N are the values of truncation terms ; m and n are serial numbers, and A_{ij} is the undetermined expansion coefficient ; the harmonic factor e^{iwt} represents the function of the displacement of the thin-walled part with time. $\varphi_i(x)$ and $\varphi_j(y)$ are the function expressions along the x and y directions respectively:

$$\phi_i(x)=\begin{array}{ll} (1-\frac{x}{l_x})^s, & s=1,2 \\ x(l_x-x), & s=3 \\ \sin\frac{s\pi x}{l_x}, & s\geqslant 4 \end{array} \tag{3}$$

$$\varphi_j(y)=\begin{array}{ll} (1-\frac{y}{l_y})^r, & r=1,2 \\ y(l_y-y), & r=3 \\ \sin(\frac{r\pi y}{l_y}), & r\geqslant 4 \end{array} \tag{4}$$

Under clamping conditions, the potential energy V_0 of the thin-walled part includes the bending strain energy V_p and the spring elastic potential energy V_S.

$$V_0=V_p+V_s \tag{5}$$

Without any excitation, the energy functional of thin-walled parts can be expressed as:

$$\Pi=T_0+V_0=T_0+V_p+V_s \tag{6}$$

Use the variational method to take the extreme value of the energy functional of thin-walled parts:

$$\frac{\partial \Pi}{\partial A_{ij}}=\frac{\partial T_0}{\partial A_{ij}}+\frac{\partial V_p}{\partial A_{ij}}+\frac{\partial V_s}{\partial A_{ij}}=0 \tag{7}$$

Substituting formula (1), formula (5) and formula (6) into formula (7), we get:

$$\left(\mathbf{K}-\omega^2\mathbf{M}\right)\mathbf{A}=0 \tag{8}$$

In the formula, K represents the total potential energy stiffness matrix of the thin-walled part; M represents the mass matrix of the thin-walled part; A is the unknown Fourier series matrix. The Rayleigh-Ritz energy variation method is used to simplify the dynamic structure problem of thin-walled parts into the problem of solving the eigenvalues of equation (8).

2.2 Prediction method for dynamic characteristics of thin-walled parts considering time-varying stiffness

Based on the free vibration model of thin-walled parts under initial working conditions established for different clamping conditions, a prediction method for the dynamic characteristics of thin-walled parts considering the time-varying stiffness during milling is proposed. Changes in mass during the milling process will cause corresponding changes in energy. The kinetic energy and potential energy after milling can be expressed as:

$$T_{rm}=T_0-\Delta T \tag{9}$$

$$V_{rm}=V_0-\Delta V \tag{10}$$

In the formula,ΔT and ΔV represent the changing kinetic energy and potential energy during the milling process.

A set of eigenvalues λ_i can be obtained by solving equation (8). The eigenvectors corresponding to the eigenvalues can be sorted to obtain the matrix **U**, which is the mode shape. The coordinate transformation of the displacement equation of the thin-walled part can be written as:

$$\mathbf{w}(t)=\mathbf{U}_0\mathbf{P}_0(t) \tag{11}$$

In the formula, **P** represents the modal coordinate vector.

The $\mathbf{M}_0$ and $\mathbf{K}_0$ matrices under initial working conditions are:

$$\mathbf{M}_0=\frac{1}{2}\rho h\int_S \dot{\mathbf{U}}\dot{\mathbf{U}}^{\mathrm{T}}\,\mathrm{d}s \tag{12}$$

$$\mathbf{K}_0=\frac{D}{2}\int_S V_p(\mathbf{U})\mathrm{d}s+\frac{1}{2}V_s(\mathbf{U}) \tag{13}$$

M and **K** under the m-th tool position are expressed as:

$$\mathbf{M}_m=\mathbf{M}_{m-1}-\Delta\mathbf{M}=\mathbf{M}_{m-1}-\frac{1}{2}\rho\Delta h\int_{\Delta S_m}\dot{\mathbf{U}}\dot{\mathbf{U}}^{\mathrm{T}}\,\mathrm{d}s \tag{14}$$

$$\mathbf{K}_m=\mathbf{K}_{m-1}-\Delta\mathbf{K}=\mathbf{K}_{m-1}-\frac{D_{rm}}{2}\int_{\Delta S_m}V_P(\mathbf{U}_m)\mathrm{d}s \tag{15}$$

The undamped free vibration equation of thin-walled parts can be written as:

$$\mathbf{M}_m\ddot{\mathbf{w}}(t)+\mathbf{K}_m\mathbf{w}(t)=0 \tag{16}$$

During the milling process, $\mathbf{M}_m$ and $\mathbf{K}_m$ of thin-walled parts can be composed of $\mathbf{M}_0$ and $\mathbf{K}_0$ under the initial working conditions and the changing $\Delta\mathbf{M}$ and $\Delta\mathbf{K}$, which can be expressed as:

$$\begin{aligned}\mathbf{M}_m&=(\mathbf{M}_0+\Delta\mathbf{M})\\ \mathbf{K}_m&=(\mathbf{K}_0+\Delta\mathbf{K})\end{aligned} \tag{17}$$

Substitute equation (17) into equation (16):

$$(\mathbf{M}_0+\Delta\mathbf{M})\ddot{\mathbf{w}}(t)+(\mathbf{K}_0+\Delta\mathbf{K})\mathbf{w}(t)=0 \tag{18}$$

Multiply the modal shape matrix in the milling process on the left side of equation (18), and substitute equation (11) into:

$$\mathbf{U}_m^{\mathrm{T}}(\mathbf{M}_0+\Delta\mathbf{M})\mathbf{U}_m\ddot{\mathbf{P}}_m(t)+\mathbf{U}_m^{\mathrm{T}}(\mathbf{K}_0+\Delta\mathbf{K})\mathbf{U}_m\mathbf{P}_m(t)=0 \tag{19}$$

In order to simplify the system dynamics equation, modal decoupling is performed:

$$\mathbf{U}_m^{\mathrm{T}}(\mathbf{M}_m+\Delta\mathbf{M})\mathbf{U}_m=\mathbf{I} \tag{20}$$

$$\mathbf{U}_m^{\mathrm{T}}(\mathbf{K}_m+\Delta\mathbf{K})\mathbf{U}_m=\boldsymbol{\omega}_m^2 \tag{21}$$

The mass matrix **M** and stiffness matrix **K** use the mode shape of the structure to convert from the general complete form to the diagonal form, which simplifies the complexity of the problem.

$$\ddot{\mathbf{P}}_m(t)+\boldsymbol{\omega}_m^2\mathbf{P}_m(t)=0 \tag{22}$$

However, actual systems have certain damping. After preliminary modal analysis, the damping ratio is introduced to simulate the actual situation more accurately.

$$\ddot{\mathbf{P}}_m(t)+2\xi_m\boldsymbol{\omega}_m\mathbf{P}_m(t)+\boldsymbol{\omega}_m^2\mathbf{P}_m(t)=0 \tag{23}$$

The mirror image processing system consists of a support head and a milling cutter. The two are in a mirror image relationship and move synchronously to complete the milling process, as shown in Figure 2.

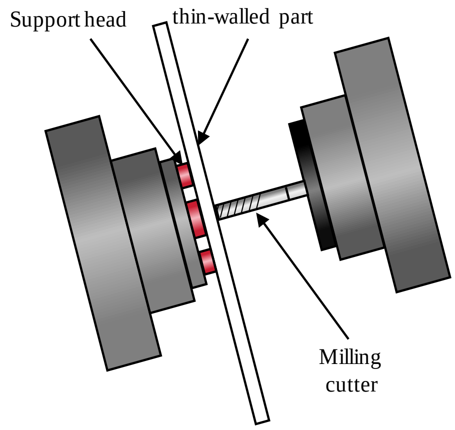

Figure 2 Principle diagram of mirror milling processing

The instantaneous load F on the thin-walled part at time t consists of the support force $\mathbf{F_s}$ and the milling force $\mathbf{F_m}$:

$$\mathbf{F}(t)=\mathbf{F_s}(t)+\mathbf{F_m}(t) \tag{24}$$

Therefore, the dynamic equation during the milling process in the modal space can be expressed as:

$$\ddot{\mathbf{P}}_m(t)+2\xi_m\boldsymbol{\omega}_m\mathbf{P}_m(t)+\boldsymbol{\omega}_m^2\mathbf{P}_m(t)=\mathbf{U}_m^{\mathrm{T}}\mathbf{F}(t) \tag{25}$$

The damping ratio can be measured through modal experiments, and the frequency response function of the thin-walled part at the m-th tool position can be calculated through equation(25).

3 Experimental procedures

Data processing uses the DASP software of Beijing Oriental Vibration and Noise Technology Research Institute，The hammering mode experiments of the workpiece were carried out under the initial working conditions, under the action of support force and after milling (the edge length of the processed square grid is 100mm×100mm, the cutting depth is 0.5mm). The clamping method is symmetrical clamping, and the sensor On the same side of the measuring point, The layout of sensors and excitation points is shown in Figures 3. The excitation device and signal acquisition device use the 085D05 type force hammer and the INV9822 type acceleration sensor. The sampling frequency is 1024Hz. Finally, the experimental data are processed and analyzed.

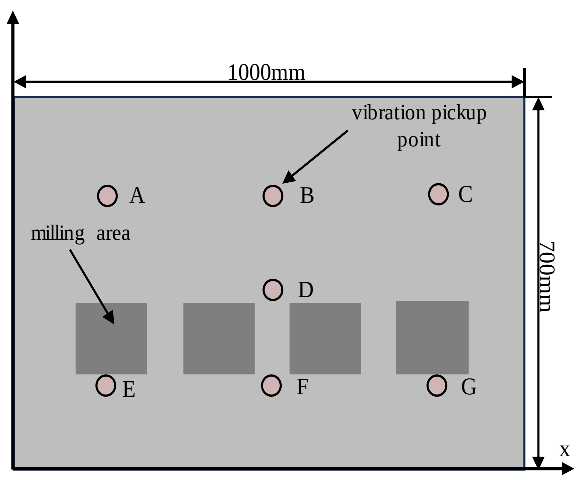

Figure 3 Schematic diagram of excitation point layout and milling area

The frequency response function image can directly reflect the change in stiffness under the influence of the support head and material removal. Under unsupported conditions, the position of point D is the location where thin-walled parts easily vibrate, so the experimental data of point D is selected as the observation point. Figure 4 is a comparison of theoretical predictions and experimental data for thin-walled parts under different conditions. From Figure 4, it can be seen that within 0 to 600Hz, the theoretical predictions and experimental FRF of thin-walled parts under initial operating conditions are basically consistent. There are small errors in amplitude and frequency, which are analyzed to be due to insufficient introduction of constraint stiffness in the theoretical prediction model, which affects the calculation results.

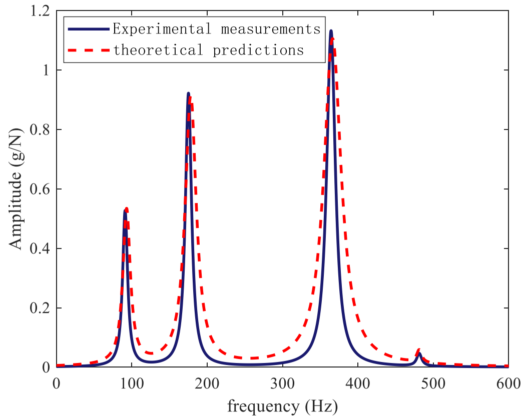

Figure 4 FRF of thin-walled parts under initial working conditions

Figure 5 The amplitude of the third-order natural frequency of the thin-walled part under the support condition is 62.72% smaller than the amplitude of the thin-walled part under the initial working condition. The amplitude predicted by the theoretical prediction is greater than the experimental result because the theoretical model introduces the support head. Caused by the lower damping value. Compared with the initial working conditions in picture Figure 6, when supports are introduced, the amplitude of acceleration of thin-walled parts is significantly reduced. When the vibration frequency is the first-order natural frequency, the theoretical prediction value and experimental measurement value under the initial conditions are 0.451g respectively 0.436g/N. The theoretical prediction value and experimental measurement value under support conditions are 0.083g/N and 0.081g/N respectively. After adding support, the acceleration amplitude reduced by the theoretical prediction value and experimental measurement value is 81.6% respectively. , 81.4%; when the vibration frequency is at the second-order natural frequency, the theoretical prediction value and experimental measurement value under initial conditions are 0.739g/N and 0.714g/N respectively, and the theoretical prediction value and experimental measurement value under support condition are 0.255 respectively. g/N, 0.232g/N, after adding supports, the acceleration amplitudes reduced by the theoretical prediction value and experimental measurement value are 65.5% and 67.5% respectively; when the vibration frequency is at the third-order natural frequency, the theoretical prediction value and experimental value under initial conditions The measured values are 1.012g/N and 0.993g/N respectively. The theoretical predicted values and experimental measured values under support conditions are 0.425g/N and 0.373g/N respectively. The theoretical predicted values and experimental measured values decrease in acceleration after adding supports. The amplitudes are 58.0% and 61.70% respectively; in addition, according to the data in Table 1, the natural frequency also increases slightly under the support condition. The first three steps increase by 3.29Hz, 2.85Hz and 3.31Hz respectively, with the increase rates of 3.9% and 1.6 respectively. %, 0.8%. The above phenomenon shows that the error between the theoretical prediction results and the actual measured values is small. The intervention of the support increases the mass of the thin-walled part and the stiffness of its location, and the damping effect it carries effectively suppresses the vibration response of the thin-walled part.

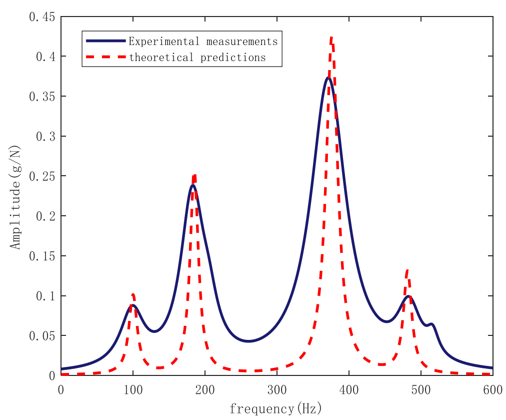

Figure 5 FRF of thin-walled parts under 100N support force

In Figure 6, the theoretical prediction has a small error compared with the experimentally measured amplitude. In addition to the error in Figure 6, it is also related to the over-idealization of material removal in the theoretical model. Compared with Figure 6, from experimental measurements and theoretical data, the amplitude of the third-order natural frequency increased by 12.35%. The increase in FRF amplitude after milling is due to the reduction in stiffness of thin-walled parts caused by material removal.

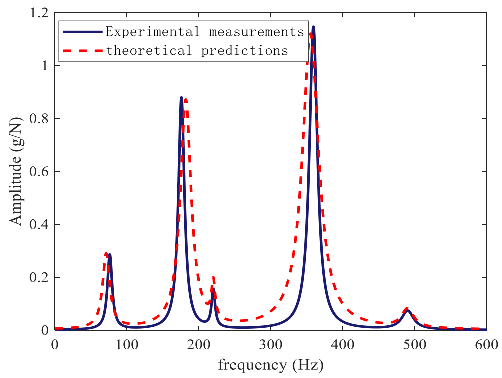

Figure 6 FRF of a thin-walled part after milling an area

4 Results

This article focuses on the clamping method of large thin-walled parts, based on the improved Fourier series, using springs with different stiffnesses to simulate boundary conditions, and then solves the kinetic energy, potential energy and elastic elastic potential energy of the thin-walled parts under the initial working conditions. Use the variational method to perform functional extremum to obtain its natural frequency. Considering the changes in the quality of thin-walled parts and the influence of the support head during the milling process, the stiffness matrix was iteratively calculated, a dynamic model was established, and the accuracy of the model was verified through experiments, and the following conclusions were drawn:

The intervention of the support has a great influence on the amplitude of mirror milling. When the support force is applied, the local stiffness of the support part increases and the amplitude decreases. Compared with the amplitude of the initial working condition, it has a significant inhibitory effect; as the milling area increases, the thinning The overall stiffness of the wall parts decreases, the natural frequency decreases and the amplitude increases compared with the initial working condition. Considering the impact of time-varying stiffness on vibration helps to improve the machining accuracy.

About the Author

Xingguo Chang, Master Student, Intelligent Manufacturing and Precision Machining.

References

[1] Karimi, Behnam, and Yusuf Altintas. "Hybrid modeling of position-dependent dynamics of thin-walled parts using shell elements for milling simulation." Journal of Manufacturing Science and Engineering 144.8 (2022): 081014.

[2] Xiao J L , Zhang Q Y , Liu H T ,et al.Research on vibration suppression by a multi-point flexible following support head in thin-walled parts mirror milling[J].International Journal of Advanced Manufacturing Technology, 2020, 106(2).

[3] Li, XiangFei, et al. "A review of recent advances in machining techniques of complex surfaces." Science China Technological Sciences 65.9 (2022): 1915-1939.

[4] Bao, Yan, et al. "Model for surface topography prediction in mirror-milling of aircraft skin parts." The International Journal of Advanced Manufacturing Technology 95 (2018): 2259-2268.

[5] Cui Huiting, Chen Weifang, Feng Ting. Research on clamping optimization to suppress vibration in thin-walled parts processing [J]. Combined Machine Tools and Automated Processing Technology, 2016, (5): 138-142.

[6] Li Liang. Processing vibration analysis and processing technology research of thin-walled parts [D]. Nanjing University of Aeronautics and Astronautics, 2005.

[7] Zhang Jun, Li Tianyun, Zhu Xiang, et al. Analysis of self-vibration characteristics of complex-shaped planar thin plates based on the improved Rayleigh-Ritz method [J]. Vibration and Impact, 2019, 38(19): 45-51

[8] Wan Chunbo, Ju Changyu, Zhang Yibo, etc. Research on chatter stability prediction in thin-walled parts milling [C]//China Association for Science and Technology Aviation Engine Industry-Academic Consortium, China Aerospace Power Federation. The 6th Aerospace Power Federation Proceedings of the Conference and the 42nd Technical Exchange Conference of the Third Professional Information Network of China Aerospace Industry (Volume 7). Beijing Institute of Power Machinery; Northeastern University, 2022:11.

[9] Arnaud L , Gonzalo O , Sébastien Seguy, et al. Simulation of low rigidity part machining applied to thin-walled structures[J]. International Journal of Advanced Manufacturing Technology, 2011, 54(5-8):479-488.

[10] Bo Q , Liu H , Lian M ,et al.The influence of supporting force on machining stability during mirror milling of thin-walled parts[J].Springer London, 2019(9).